

# Low-Temperature Preparation of Single Crystal Titanium Carbide Nanofibers in Molten Salts

Xuanke Li,<sup>\*,†,‡,§</sup> Zhijun Dong,<sup>†,§</sup> Aidan Westwood,<sup>‡</sup> Andy Brown,<sup>‡</sup> Rik Brydson,<sup>‡</sup> Alex Walton,<sup>#</sup> Guanming Yuan,<sup>§</sup> Zhengwei Cui,<sup>§</sup> and Ye Cong<sup>§</sup>

<sup>†</sup>High Temperature Ceramic and Refractory Key Laboratory of Hubei Province, Wuhan University of Science and Technology, Wuhan, Hubei 430081, P. R. China

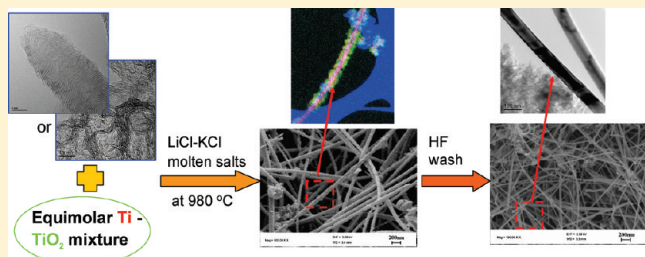
<sup>‡</sup>Institute for Materials Research, School of Process, Environmental and Materials Engineering, University of Leeds, Leeds, LS2 9JT, U.K.

<sup>§</sup>The Hubei Province Key Laboratory of Coal Conversion and New Carbon Materials, Wuhan University of Science and Technology, Wuhan, Hubei 430081, P. R. China

<sup>#</sup>School of Physics and Astronomy, University of Leeds, Leeds, LS2 9JT, U.K.

 Supporting Information

**ABSTRACT:** The synthesis of single crystal titanium carbide (TiC) nanofibers has been investigated by the reaction of carbon sources of various sizes and microstructures with an equimolar mixture of titanium dioxide ( $TiO_2$ ) and titanium metal powders, in a molten salt medium. The carbon sources included carbon lamp black, thermal carbon black, pyrolytic carbon black, and multiwalled carbon nanotubes (MWCNTs). The reaction of titanium with  $TiO_2$  in molten salt to form titanium monoxide and the absence of reaction of titanium oxides with carbon nanotubes in molten salt is also reported. A reasonable yield of single crystal TiC nanofibers can only be achieved with the pyrolytic carbon black and MWCNT carbon sources. The product needs purification in hydrofluoric acid to remove  $TiO_2$  surface contamination. Four-point electrical measurement of a purified nanofiber in a dual scanning electron microscope-scanning tunneling microscope (SEM-STM) nanoprobe confirms the stoichiometry  $TiC_x$  to be  $x = 0.95$ . The results suggest that critical factors in the formation of single crystal TiC nanofibers in molten salts are that the carbon source should contain graphitic material and possess a length-scale in the nanometer range and that a near equimolar mixture of  $TiO_2$  and Ti is used.



## 1. INTRODUCTION

Titanium carbide (TiC) is one of the most important metal carbides used in the field of wear resistant tools and in the aerospace material industries. TiC has a high melting temperature (3067 °C), high Young's modulus (410–450 GPa), high Vickers hardness (28–35 GPa),<sup>1,2</sup> high chemical stability, and good thermal and electrical conductivities.<sup>3,4</sup> Single crystals of TiC have been developed as stable field emitters<sup>5</sup> because they have a low work function and low volatility.

Many methods for growing single crystals of this compound have been reported. Single crystals of titanium carbide have been prepared by the Verneuil technique,<sup>6,7</sup> a floating zone process,<sup>5,8,9</sup> precipitation from molten metals,<sup>10</sup> and chemical vapor deposition.<sup>11–14</sup> It has been reported that TiC, SiC, NbC, and TaC nanorods could be obtained in metal oxide/metal halide vapor–solid reactions using carbon nanotubes as a template material.<sup>15</sup> These syntheses are difficult since they require high temperatures and/or rigorous handling of volatile/highly reactive reagents.

In our previous work,<sup>16</sup> we found that single crystal TiC nanofibers were produced at a relatively low temperature of 950 °C by reaction of a mixture of titanium (Ti) with multiwalled

carbon nanotubes (MWCNTs) in a molten salt medium composed of LiCl-KCl-KF. We also reported that the yield of single crystal TiC nanofibers could be significantly enhanced by using an equimolar titanium dioxide ( $TiO_2$ )/Ti mixture instead of Ti powder alone. We speculated that this may be for a couple of reasons: because the oxide represents a less active source of titanium than the metal, allowing more gradual, single crystal growth to occur epitaxially on short lengths of the MWCNT; or that a derivative suboxide or possibly defective suboxide such as cubic titanium monoxide (TiO) or an oxycarbide may act as a preferential nucleation site for the carbide formation. Liu and Zhang<sup>17</sup> have demonstrated polycrystalline, nanoparticulate, TiC coating of graphite flakes using a similar molten salt process with just Ti powder as the metal precursor, also inferring a graphitic template growth mechanism. In a subsequent publication,<sup>18</sup> these authors discuss evidence for the solubility of Ti powder in the molten salt mixture. They suggest that the salt medium potentially facilitates the

**Received:** March 27, 2011

**Revised:** May 24, 2011

**Published:** May 27, 2011

dissolution, dispersion, and transport of Ti to the surface of the graphite for subsequent reaction. Also, they demonstrate that the synthesis does not require addition of KF to the salt mixture, unlike Liu and Zhang<sup>17</sup> and Li et al.<sup>16</sup> who did include KF.

This work reports the synthesis and characterization of single crystal TiC prepared by reaction of various separate graphitic carbon sources (of different morphologies), with a mixture of Ti with  $\text{TiO}_2$  in a LiCl-KCl molten salt reaction medium (without addition of KF). The reaction of Ti with  $\text{TiO}_2$  in molten salt and the unreactivity of titanium oxides alone with carbon nanotubes in molten salt are also reported. The objective of this work is to show the influence of size and microstructure in graphitic carbon sources on the formation and quality of single crystal TiC nanofibers. Potential nucleation mechanisms will also be discussed.

## 2. EXPERIMENTAL SECTION

Four sources of graphitic carbon with very different microstructures and morphologies were employed: three carbon blacks (lamp carbon black, thermal carbon black, pyrolytic carbon black) and MWCNTs. The lamp carbon black and the thermal carbon black were provided by the Morgan Crucible Company in the UK. The pyrolytic carbon black was purchased from Zibo Huaguang chemical plant in China. Powder X-ray diffraction patterns and thermogravimetric analysis of these carbon black materials are reported in the Supporting Information. The MWCNTs were prepared in-house by a catalytic chemical vapor decomposition method.<sup>19</sup> An equimolar mixture of  $\text{TiO}_2$  and Ti powders was used as the titanium source. Titanium dioxide with purity 99.5% was purchased from J&K Scientific Ltd. in China. Titanium powder (ca. 300 mesh and purity above 99.9%) was purchased from Beijing Mountain Technical Co. Ltd. in China. The single crystal TiC nanofibers were synthesized by reacting the carbon and titanium sources at a 2:1 (C/Ti) molar ratio in a molten salts mixture. The mass ratio between the molten salts mixture and the carbon plus  $\text{Ti}/\text{TiO}_2$  mixture was about 9:1.

Each carbon source was dispersed in trichloromethane using ultrasonic vibration for 15 min and then mixed with the salts and the equimolar mixture of  $\text{TiO}_2$  and Ti powders, which had been dried for several hours in an oven at 100 °C. The salt mixture was composed of LiCl and KCl in eutectic quantities (LiCl/KCl = 58.8:41.2 mol %). This mixture was placed in a covered alumina crucible and reacted at 980 °C for 5 h under a flowing argon atmosphere. After cooling, the crucible was repeatedly boiled in fresh aliquots of water to remove the salts and excess carbon by decanting. The remaining product was dried at 50 °C for 12 h. Purification of the remaining product was carried out by treatment with hydrofluoric (HF) acid under magnetic stirring for 24 h to remove the  $\text{TiO}_2$  within the reaction product, particularly on the surface of the resulting TiC nanofibers. Finally, the sample was thoroughly washed in water in order to neutralize the specimen.

In order to provide information on product microstructure and elemental composition, following initial examination by scanning electron microscopy (SEM), high resolution transmission electron microscopy (HRTEM), selected-area electron diffraction (SAED), and electron energy loss spectroscopy (EELS) analyses were conducted on representative sample areas. TEM samples were prepared by ultrasonic dispersion of the powder products in alcohol, dropping onto a standard TEM holey carbon support film (Agar Scientific) and then drying in air. The specimens were examined with a Philips CM200 field emission gun-TEM operating at 197 kV and fitted with a Gatan imaging filter (GIF 200) and Oxford Instruments UTW ISIS X-ray detector. The electron diffraction patterns were indexed against the International Centre for Diffraction Data (ICDD) inorganic compound powder diffraction file database in order to identify the crystalline phases present.

Electrical transport measurements were performed on the purified TiC nanofibers in an Omicron Nanoprober, comprised of four independently controlled scanning tunnelling microscope (STM) tips under

a high resolution SEM in an ultra high vacuum chamber. A drop of nanofiber suspension was placed onto a piece of clean silicon and the solvent was allowed to evaporate, leaving the nanofibers dispersed on the silicon. The use of a silicon substrate allowed the tips to be brought into tunnelling contact with its surface using STM feedback loops with a large gap voltage ( $V_{\text{gap}} > 6$  V). From this tunnelling contact, the feedback loops were disconnected and the tips were then moved laterally into contact with a nanofiber. The silicon substrate was many orders of magnitude less conductive than the nanofibers, and furthermore the tungsten tip/nanofiber interface formed a Schottky barrier, so conduction between the tips through the silicon substrate was negligible.<sup>20</sup> Transport measurements were taken with the four STM tips in a colinear arrangement. The outer tips were used to source a current through the nanofiber. The potential difference was measured between the two inner tips. By varying the separation of the inner tips between successive measurements, the variation of resistance with length could be determined. A Keithley 2400 sourcemeter was used as the current source. One Keithley 6514 electrometer was placed in series with the sourcemeter and measured the current through the outer tips. Another Keithley 6514 electrometer measured the potential difference between the inner tips.

## 3. RESULTS AND DISCUSSION

The SEM and TEM images shown in Figure 1a–d are representative of the morphology of carbon lamp black, thermal carbon black, pyrolytic carbon black, and MWCNTs, respectively. The lamp, thermal, and pyrolytic carbon blacks consist of agglomerates of primary particles that are spherical and have diameters in the range 110–300 nm, 120–500 nm, and 20–40 nm, respectively (Figure 1a–c). The diameter and length of the carbon nanotubes are around 15–40 nm and a few micrometers, respectively (Figure 1d). The diameters of the pyrolytic carbon black particles and the MWCNTs are similar and much smaller than those of the carbon lamp black and the thermal carbon black particles. Figure 1a,b shows that both the carbon lamp black and thermal carbon black are composed of solid spherical particles. The pyrolytic carbon black and MWCNTs shown in Figure 1c,d display a low density center indicating a hollow ball and hollow fiber microstructure, respectively.

Figure 2 shows the TEM atomic lattice images of the (a) carbon lamp black, (b) thermal carbon black, (c) pyrolytic carbon black, and (d) MWCNTs. The images confirm that all the carbon sources are composed of turbostratic graphitic material. The insets in Figure 2a–d are the magnified images of the lattice fringes from within the marked boxes in Figure 2a–d, respectively. The intergraphene spacing of ca. 0.35 nm for the {002} plane of graphitic carbon can be readily resolved in these images. The edges of the nanosized pyrolytic carbon black and MWCNTs (Figure 2c,d) are more ordered and display a less turbostratic structure and herringbone structure, respectively, in comparison to the former two carbon blacks. The poorly ordered, graphitic nature, and purity of these carbon blacks was confirmed by a combination of X-ray diffraction (XRD) and thermogravimetric analysis (Supporting Information).

The secondary electron images of the products of the reaction of (a) carbon lamp black and (b) thermal carbon black precursor materials with the equimolar mixture of  $\text{TiO}_2$  and Ti powders in molten salt are shown in Figure 3, panels a and b, respectively. The SEM observation (Figure 3) indicates that the straight nanofibers within the product seem to be covered by some nanosized particles. Figure 3a,b clearly shows that few straight, fibrillar materials are produced from the lamp black and thermal carbon black precursors. Comparison of these carbon black-derived products (Figure 3a,b), with the materials produced from the pyrolytic carbon black and MWCNT precursors (Figure 3c,d), reveals that significantly more

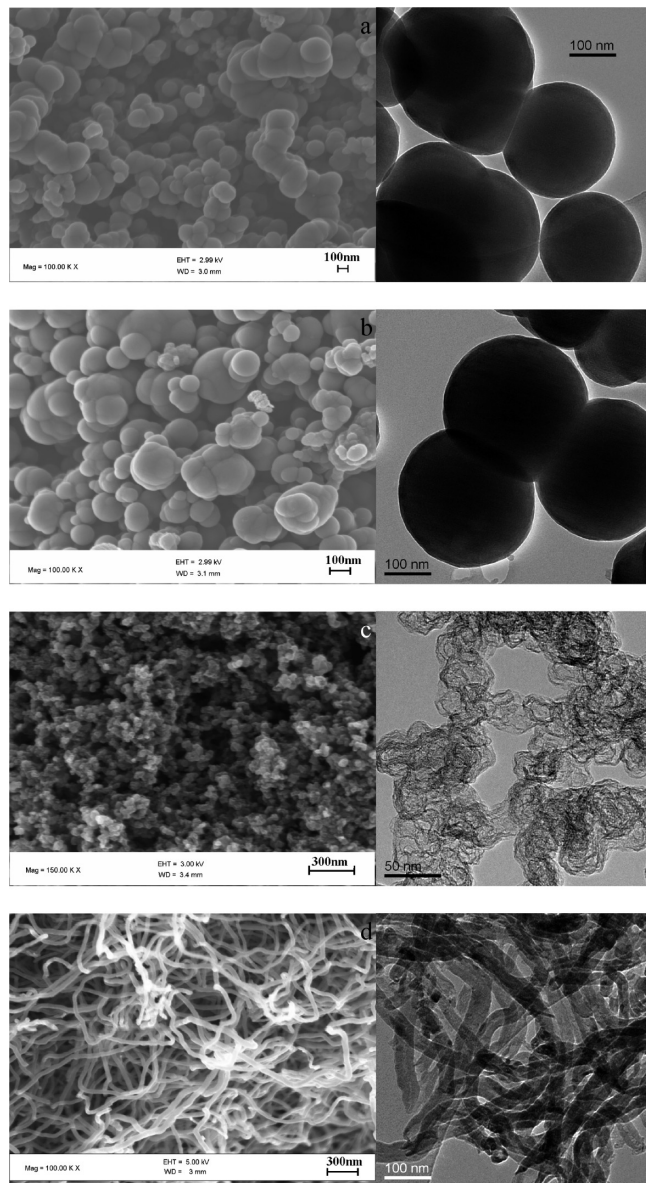


**Figure 1.** Typical SEM and TEM images of (a) carbon lamp black, (b) thermal carbon black, (c) pyrolytic carbon black, and (d) MWCNTs.

straight nanofibers are present in the latter materials. Although it is difficult to quantify the exact yield, SEM observation of many sample regions suggests that the yield is reasonable. Furthermore, the distinctive morphology of unreacted carbon black is evident in the images of the lamp black and thermal carbon black-derived material (cf. Figure 3a,b with Figure 1a,b, respectively). In contrast, there is little or no retention of precursor morphology in the pyrolytic carbon black and MWCNT-derived product (cf. Figure 3c,d with Figure 1c,d, respectively). It will be confirmed by TEM and XRD (shown below) that the nanofibers visible in the SEM images are indeed composed of TiC. If the formation of single crystal TiC nanofibers results from the dissolution, transport, and homogeneous nucleation of the carbon and titanium sources within the liquid phase molten salt medium or via nucleation on a Ti suboxide, it should be possible to form single crystal TiC nanofibers from any of the various carbon sources. Instead, it is observed that the significant difference between the morphologies of the carbon precursors affects the formation of

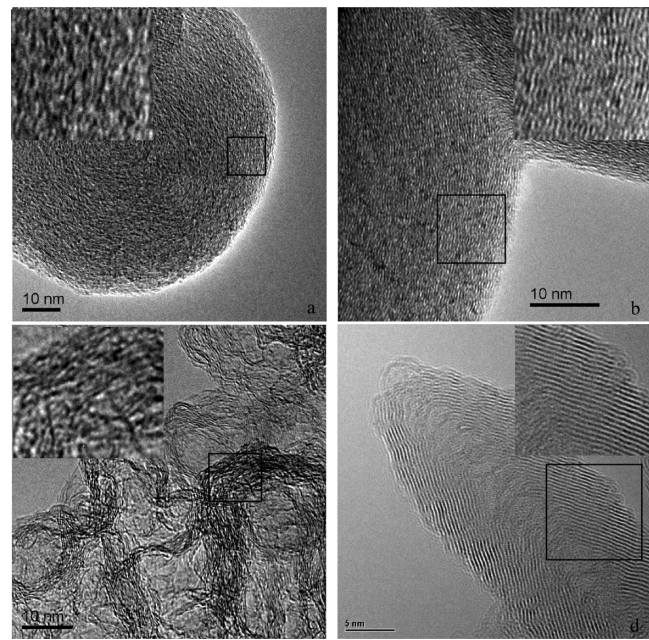


**Figure 2.** Typical HRTEM images of (a) carbon lamp black, (b) thermal carbon black, (c) pyrolytic carbon black, and (d) MWCNTs; the insets in (a–d) are the magnified images from the corresponding box shown in panels a–d. The lattice fringes have spacing consistent with the {002} intergraphene plane of graphitic material and the curvature and waviness of the planes indicate a turbostratic structure.

the straight single crystal TiC nanofibers. The larger, more disordered lamp black and thermal carbon black materials produce small amounts of TiC fibers compared to the pyrolytic carbon black and MWCNTs. A carbon source with appropriate crystallinity and/or size seems to be a key factor for what appears to be the heterogeneous growth of single crystal TiC nanofibers.

Figure 4a shows the TEM bright field image of a nanofiber derived from the pyrolytic carbon black, before purification by HF acid treatment. It indicates that the nanofiber is coated by some fine particles. The inset in Figure 4a shows the corresponding SAED pattern which displays diffraction rings indexable to the {101}, {103}, {105}, {213}, and {107} planes of  $\text{TiO}_2$  (anatase). The relative intensities of the rings in the SAED pattern are similar to the standard XRD intensities for anatase (ICDD database reference code: 00-001-0562). The spots in the pattern are indexable to cubic TiC (ICDD database reference code: 01-089-3828). A TEM atomic lattice image of the coated TiC nanofiber is shown in Figure 4b. Crystalline fringes of various orientations can be identified in Figure 4b, and the spacings confirm that the nanocrystals which coat the fiber are composed of  $\text{TiO}_2$ . In order to ensure differentiation between the titanium dioxide particle coating and the TiC nanofiber core, energy filtered TEM (EF-TEM) jump ratio images at the oxygen K-edge, titanium  $L_{2,3}$ -edge and carbon K-edge of the nanofiber (shown in Figure 4a) were recorded (Figure 4, panels c–e, respectively). EF-TEM is a powerful tool that can be used to acquire elemental distribution maps with high lateral resolution and short acquisition times. Oxygen and carbon rich regions shown in Figure 4c,e appear bright and are localized to the coating and core of the nanofiber, respectively. The titanium rich regions shown in Figure 4d appear to have a similar contrast and therefore uniform distribution throughout the whole nanofiber.

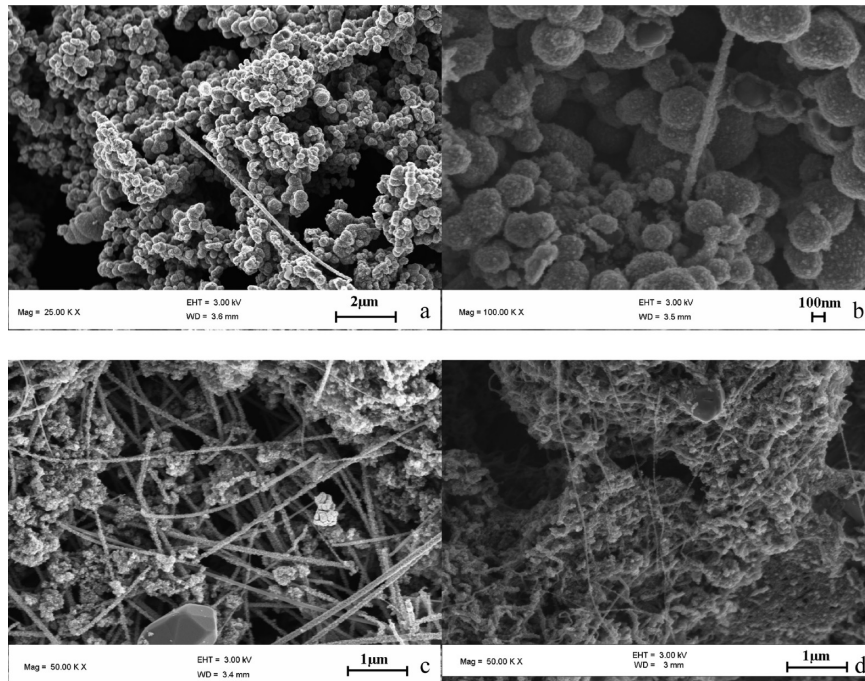


**Figure 3.** Typical SEM images of the products derived from the reaction of a mixture of  $\text{TiO}_2$  and Ti with (a) carbon lamp black, (b) thermal carbon black, (c) pyrolytic carbon black, and (d) MWCNTs in molten salts.

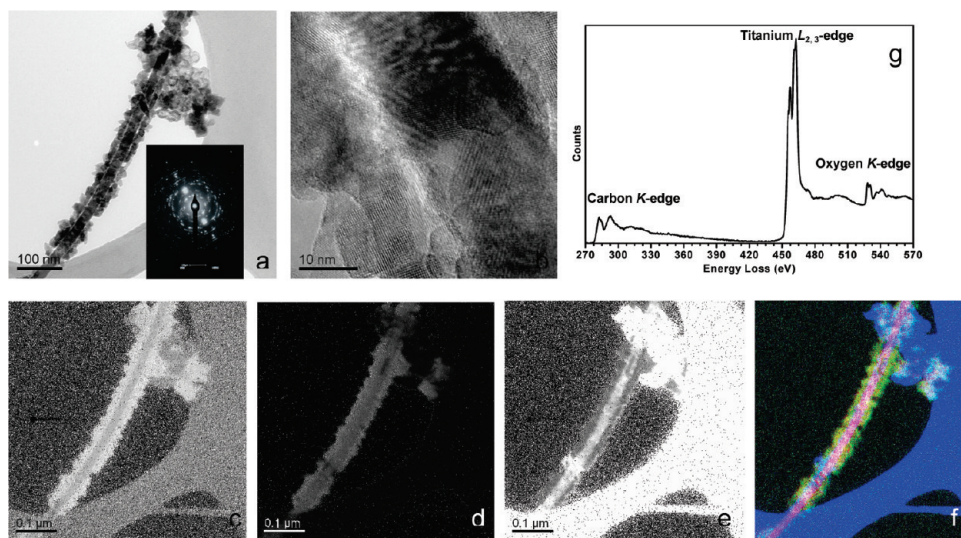


**Figure 4.** Typical EF-TEM images of unpurified single TiC nanofibers prepared from the pyrolytic carbon black precursor. (a, b) Bright field TEM images of primary single TiC nanofibers; the inset in (a) is an SAED pattern (spots indexed to cubic TiC and rings to tetragonal  $\text{TiO}_2$ ) from the fibers shown in (a). (c) Oxygen K-edge jump ratio image, (d) titanium  $L_{2,3}$ -edge jump ratio, (e) carbon K-edge jump ratio image, (f) false color map of O (green) / Ti (red) / C (blue) maps combined, and (g) EEL spectrum from the fiber.

With reference to the bright-field image in Figure 4a, it is obvious that titanium dioxide nanoparticles and titanium carbide are located on the surface and the core of the nanofiber, respectively. Figure 4f shows a false color O (green)/Ti (red)/C (blue) map of the nanofiber shown in Figure 4a, and this serves to highlight the dioxide coating and carbide core of the fiber. An EEL spectrum of this nanofiber taken in the TEM is shown in Figure 4g, it shows the carbon K-edge, titanium  $L_{2,3}$ -edge and oxygen K-edge used in the elemental mapping of this nanofiber.

An oxygen K-edge signal (onset at  $\sim 530$  eV) is obviously detectable, suggesting there is a lot of oxygen relative to carbon. It cannot be confirmed from the EEL spectrum that oxygen is absent from the single crystal carbide core of the TiC nanofiber, although the EF-TEM maps would tend to suggest this.

In our previous work, the as-produced single crystal TiC nanofibers were purified by a dilute hydrofluoric acid treatment (Figure 3c,d in ref 16). The product prepared here was purified in the same manner. Figure 5 shows the SEM images of the straight

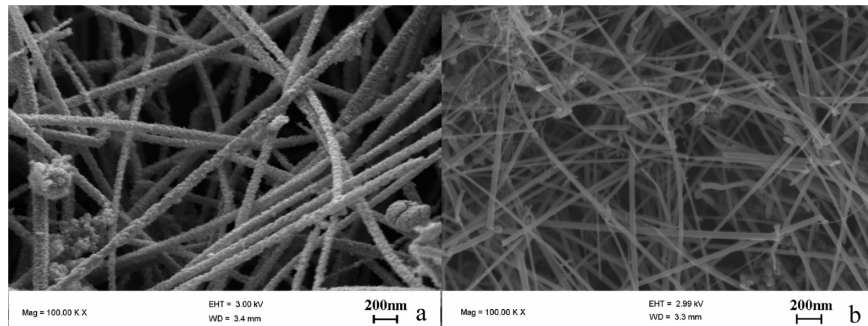


**Figure 5.** SEM images of the nanofibers prepared from pyrolytic carbon black (a) before and (b) after HF acid treatment.

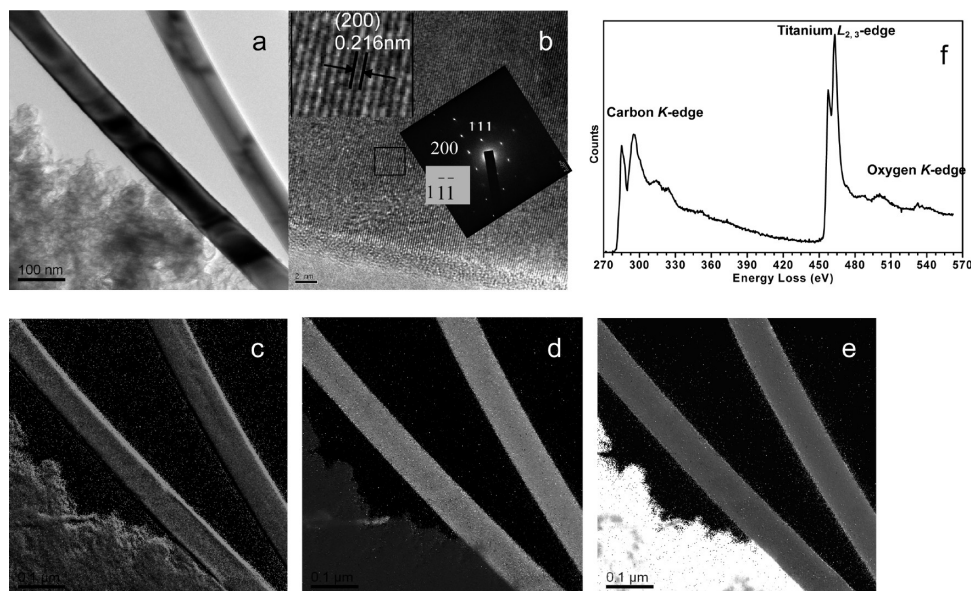


**Figure 6.** (a and b) Typical bright field TEM images of purified single TiC nanofibers prepared from pyrolytic carbon black and purified using HF acid. (c) Oxygen jump ratio image (EF-TEM), (d) titanium jump ratio image, (e) carbon jump ratio image, and (f) associated EEL spectrum. The magnified image inset in (b) is from the box in (b) showing that the lattice fringes have a spacing consistent with the  $\{200\}$  plane of the cubic TiC. The SAED pattern inset in (b) is from the fiber shown in (b).

nanofibers prepared from pyrolytic carbon black (a), before and (b), after HF acid treatment. It is observable that the straight nanofibers are of reduced diameter and smoother in morphology after HF acid purification (Figure 5b). This suggests that the titanium dioxide particle coating on the surface of the straight nanofibers has been removed. The diameter and length of the purified straight fibers are mainly 10–50 nm and tens of  $\mu\text{m}$ , respectively. Similar results were obtained for the samples derived from MWCNTs.

Figure 6a shows a bright-field TEM image of a purified nanofiber, showing that the nanofiber has a clean and smooth surface consistent with SEM images (Figure 5b). A TEM atomic lattice image of the straight nanofiber is shown in Figure 6b. The crystalline fringes (magnified and inset in b), have a spacing of 0.216 nm, consistent with the  $\{200\}$  plane spacing of cubic TiC. The SAED pattern, also inset in Figure 6b, shows that the straight nanofiber consists of single crystal TiC. This indexed SAED pattern is in true orientation with respect to the major axis of the nanofiber from which it was obtained. The major axis of the fiber lies along the  $[100]$  direction. The pattern can be indexed to the 111, 200, and  $\bar{1}\bar{1}\bar{1}$  reflections in cubic TiC, consistent with the crystal viewed down the  $[01\bar{1}]$  axis.

Figure 6c–e shows the EF-TEM jump ratio images at the oxygen K-edge, titanium  $L_{2,3}$ -edge, and carbon K-edge of the nanofibers shown in Figure 6a, respectively. In comparison with Figure 4c–e, a significant change in the elemental content of the nanofiber can be easily observed, particularly in terms of oxygen content. This confirms that the titanium dioxide particles on the surface of the single crystal TiC nanofibers have been successfully removed. The EEL spectrum of the nanofiber shown in Figure 6f reveals a carbon K-edge and a titanium  $L_{2,3}$ -edge which are consistent in shape, peak position, and relative intensity with a fully stoichiometric titanium carbide phase.<sup>21,22</sup> In this case, the oxygen K-edge signal (onset at  $\sim 530$  eV) is barely detectable, suggesting there is no more than a few atom % oxygen relative to carbon in these fibers.

In order to estimate the stoichiometry of the TiC, a series of four-point electrical measurements were taken on a purified nanofiber. Figure 7a shows a SEM image of the four-probe measurement of a purified TiC nanofiber. Figure 7b shows the linear IV characteristics of the nanofiber measured under the conditions shown in Figure 7a. A total of four four-probe measurements were taken at various inner tip separations. The linear variation in observed

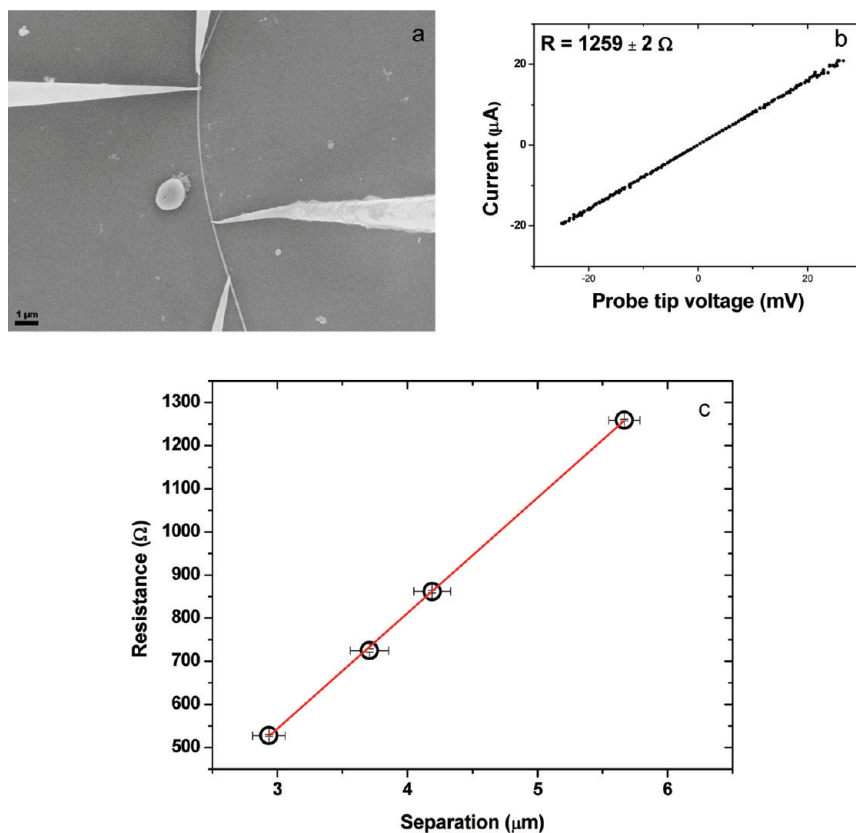


**Figure 7.** Electrical transport measurement of a purified TiC nanofiber. (a) SEM image of the four measurement probes in contact with a purified nanofiber. (b) Linear IV curve taken from the probes positioned in a; the separation of the two inner probes was measured to be  $\sim 5.7 \mu\text{m}$  and the resistance  $1259 (\pm 2) \Omega$ . (c) The linear dependence of resistance on inner probe separation, giving a resistivity value for the nanofiber of  $1.43 (\pm 0.02) \mu\Omega \text{ m}$ .

resistance could then be plotted against probe-tip separation, Figure 7c. This gave a resistivity value for the nanofiber of  $1.43 (\pm 0.02) \mu\Omega \text{ m}$ . Williams<sup>23</sup> reports the resistivity of stoichiometric TiC to be  $0.65 \mu\Omega \text{ m}$  and that resistivity increases with decreasing stoichiometry because of point defect scattering. Williams' data indicate that our nanofiber has a stoichiometry  $\text{TiC}_x$  around or slightly better than  $x = 0.95$ .

In our previous work, we demonstrated an enhanced yield of single crystal TiC nanofibers when using an equimolar mixture of  $\text{TiO}_2$  and Ti powders as a precursor.<sup>16</sup> Here, we have produced material with Ti to  $\text{TiO}_2$  molar ratios ranging from 1:1 to 4:1 and find, by SEM observation, that the equimolar ratio gives by far the highest yield of nanofibers (Supporting Information). To further explore the role the oxide plays in the formation mechanism of the single crystal TiC fibers, we have varied the powder mixing method and type of oxide content of the molten salt mixture during synthesis. Figure 8a shows a SEM image of the reaction product prepared by covering the surface of the LiCl-KCl salts/equimolar  $\text{TiO}_2$  and Ti powder mixture with MWCNTs. This is in contrast to mixing-in the MWCNTs, and then reacting this preparation under argon atmosphere at  $980^\circ\text{C}$  for 5 h. The MWCNTs were expected to remain (float) on the top of the molten salt mixture during processing. Thus, they should only react at the interface or if the  $\text{TiO}_2/\text{Ti}$  volatilized from the mixture. In practice, however, the MWCNT morphology is retained after processing and no straight nanofibers could be observed (Figure 8a). This suggests that little or no dissolution of the nanotubes occurred and that little or no contact was made

between the  $\text{Ti}/\text{TiO}_2$  mixture and the MWCNTs (i.e., the  $\text{Ti}/\text{TiO}_2$  mixture did not volatilize). This contrasts strongly with the reaction that occurred when all of the components were mixed together (Figure 3d). Clearly, once mixed, there is little propensity for the MWCNTs to separate from the mixture (by flotation) before they react. Figure 8b shows the product from attempted reaction in the molten salts of MWCNTs with only  $\text{TiO}_2$  at a molar ratio of  $\text{C}/\text{TiO}_2 = 2/1$  under an argon atmosphere at  $980^\circ\text{C}$  for 5 h. This product consists only of MWCNTs and  $\text{TiO}_2$  particles, indicating that reaction between carbon and  $\text{TiO}_2$  does not proceed in the molten salts.

$\text{TiO}$  powder was formed by a reaction of equimolar  $\text{TiO}_2$  and Ti powders in molten salts under argon atmosphere at  $980^\circ\text{C}$  for 5 h (Figure 8c). The production of  $\text{TiO}$  is confirmed by XRD analysis (Figure 8e). In order to investigate the reaction of carbon with  $\text{TiO}$  in the molten salt, the MWCNTs were mixed and processed in the molten salts, with the  $\text{TiO}$  powder at a molar ratio of  $\text{C}/\text{TiO} = 1/2$ , under the same conditions as described above. The SEM image of the product obtained from this reaction shows that no single crystal TiC nanofibers are formed (Figure 8d). This indicates that MWCNTs will not react with pure  $\text{TiO}_2$  or  $\text{TiO}$  in the molten salt medium and that titanium metal and titanium dioxide are thus crucial reagents.

These results, together with the findings of our previous work,<sup>16</sup> indicate that the addition of  $\text{TiO}_2$  to the Ti powder plus the microstructure and size of carbon precursors have a critical influence on the formation and yield of single crystal TiC nanofibers. The suggestion that the titanium powder dissolves,

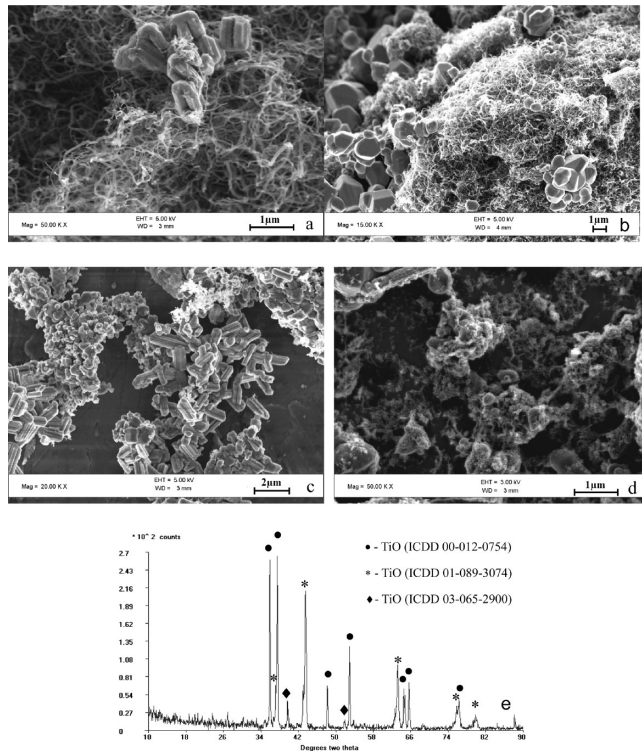


**Figure 8.** SEM images of reaction products prepared (a) by MWCNTs placed on the top of the LiCl-KCl salts and equimolar  $\text{TiO}_2/\text{Ti}$  powder mixture; (b) by attempted reaction of MWCNTs with  $\text{TiO}_2$  particles; (c) by reaction of equimolar  $\text{TiO}_2$  and Ti powders, without adding MWCNTs; (d) by reaction of MWCNTs with  $\text{TiO}$  powders; and (e) XRD pattern of  $\text{TiO}$  produced by reaction of equimolar  $\text{TiO}_2$  and Ti powders without MWCNTs.

at least partially in the molten salt,<sup>16–18</sup> seems to be supported here. A  $\text{Ti}/\text{TiO}_2$  mixture in the absence of a carbon source reacts in the molten salt to form  $\text{TiO}$  (Figure 8e). When MWCNTs are mixed with just titanium powder in the molten salt, we observe that the tubes act as templates for the formation of polycrystalline  $\text{TiC}$ .<sup>16</sup> This indicates that nucleation is dominant over growth and suggests a high availability of Ti. Presumably what growth there is proceeds in an inward manner, similar to that already observed for  $\text{TiC}$  formation on CNTs by Wong et al.<sup>24</sup> With the addition of  $\text{TiO}_2$  however, we see a switch to significant amounts of single crystal formation (Figure 3d). This is a nucleation limited process indicating a reduction in Ti availability. We suggest that this is because the additional reaction of Ti with  $\text{TiO}_2$  reduces the availability of dissolved Ti to react with the carbon. The formation of the  $\text{TiC}$  nanofibers might then proceed by a low rate of epitaxial nucleation of  $\text{TiC}$  on short lengths of graphitic material. This could occur because of the close correspondence between the graphite (100) *d*-spacing (0.213 nm) and the cubic  $\text{TiC}$  (200) *d*-spacing (0.216 nm). Alternatively, the addition of dissolved  $\text{TiO}$  onto the surface of the graphitic material (and possible disproportionation to form Ti and  $\text{TiO}_2$ ) may lead to the nucleation of carbide following reduction with the graphite. This mechanism has been put forward for the vapor phase reaction of  $\text{TiO}$  with CNTs at higher temperature (1375 °C).<sup>15</sup> While we have no firm evidence as to whether one or both of these mechanisms are operating, it may be that the latter mechanism is preferred. We observed  $\text{TiO}_2$  whiskers on the

surface of the as-treated material (Figures 3, 4, and 5a) and, although this could be a result of the oxidation of Ti or  $\text{TiO}$  postsynthesis, we have just argued that there is a low availability of Ti in the molten salt. On the other hand, Figure 8d suggests that MWCNTs will not react with pure  $\text{TiO}$  in the molten salt medium.

Regardless of the mechanism, what is clear is that a carbon source of reasonably graphitic character and sub-100 nm grain size appears to be a key factor in enabling significant single crystal titanium carbide formation. On the basis of simple geometrical arguments, carbide nucleation may occur coherently at the surface of the graphitic precursor material. Both the pyrolytic carbon black and MWCNTs (Figure 2c,d) have graphitic stack lengths of no greater than approximately 15 nm. Lengths larger than this value would be expected to lead to a breakdown in interfacial coherency (based on the lattice mismatch between graphite (100) and  $\text{TiC}$  (200) spacings) and the formation of separate  $\text{TiC}$  crystals, as observed in the case of  $\text{TiC}$  nucleation on graphite flakes.<sup>17</sup> In addition, previous work, in the absence of metals, has demonstrated denuded carbon nanotube walls when treated in a molten salt mixture at high temperature.<sup>25</sup> It may be this structural breakdown of graphitic tubes/pyrolytic carbon black that provides sites for the nucleation of  $\text{TiC}$ . Clearly the exact growth mechanism of single crystal  $\text{TiC}$  nanofibers is still under study and remains to be confirmed unequivocally.

## 4. CONCLUSIONS

Single crystal  $\text{TiC}$  nanofibers were produced by the reaction of a mixture of equimolar amounts of  $\text{TiO}_2$  and Ti with twice the molar amount of nanosized pyrolytic carbon black or MWCNTs in a molten salt medium. A reasonable yield of straight nanofibers covered by fine  $\text{TiO}_2$  nanoparticles resulted (Figure 3c,d). This was in contrast to the poor yields obtained when lamp or thermal carbon black were used as the carbon source. By treating the primary product in diluted hydrofluoric acid, single crystal  $\text{TiC}$  nanofibers possessing a clean and smooth surface were obtained with sub-100 nm diameters and lengths in the range of tens of  $\mu\text{m}$ . Electrical testing indicates that these conductive nanofibers have a stoichiometry,  $\text{TiC}_x$  around or slightly better than  $x = 0.95$ .

We have demonstrated that the size and microstructure of the carbon source and the oxide content of the titanium source can all significantly affect the formation of the single crystal  $\text{TiC}$  fibers. We conclude that a carbon source that contains graphitic material and possesses a length-scale in the nanometer range, along with a near equimolar mixture of  $\text{TiO}_2$  and Ti, are critical reagent criteria for promoting the formation of single crystal  $\text{TiC}$  nanofibers in molten salts.

## ■ ASSOCIATED CONTENT

**S Supporting Information.** Powder X-ray diffraction and thermogravimetric analysis of the precursor carbon blacks; data on varying the molar ratio of Ti to  $\text{TiO}_2$  in the molten salt synthesis; This information is available free of charge via the Internet at <http://pubs.acs.org/>.

## ■ AUTHOR INFORMATION

### Corresponding Author

\*Tel/fax: +0086 27 86556906. E-mail: xkli8524@sina.com.

**■ ACKNOWLEDGMENT**

The authors acknowledge the financial support of the National Natural Science Foundation of China (Project S0672070, Project S0972110, and Project 20803054), and the Nano-Manufacturing Institute, University of Leeds.

**■ REFERENCES**

- (1) Storms, E. K. *The Refractory Carbides*; Academic Press: New York, 1967.
- (2) Pierson, H. O. *Handbook of Refractory Carbides and Nitrides*; Noyes Publications: Westwood, 1996.
- (3) Chen, Y. J.; Li, J. B.; Zhai, H. Z. *J. Cryst. Growth* **2001**, *224*, 244–250.
- (4) Khyzhun, O. *J. Alloys. Compd.* **1997**, *259*, 47–58.
- (5) Kumashiro, Y.; Itoh, A.; Misawa, S. *J. Less-Common Metals* **1973**, *32*, 21–37.
- (6) Williams, W. S. *J. Appl. Phys.* **1961**, *32*, 552–554.
- (7) Hollox, G. E.; Smallman, R. E. *J. Appl. Phys.* **1966**, *37*, 818–823.
- (8) Precht, W.; Hollox, G. E. *J. Cryst. Growth* **1968**, *3–4*, 818–823.
- (9) Storey, R. N.; Laudise, R. A. *J. Cryst. Growth* **1970**, *6*, 261–265.
- (10) Packer, M. E.; Murray, M. J. *J. Cryst. Growth* **1972**, *16*, 240–248.
- (11) Higashi, I.; Takahashi, Y.; Atoda, T. *J. Cryst. Growth* **1976**, *33*, 207–211.
- (12) Zergioti, I.; Hatziapostolou, A.; Hontzopoulos, E.; Zervaki, A.; Haidemenopoulos, G. N. *Thin Solid Films* **1995**, *271*, 96–100.
- (13) Bisch, C.; Nadal, M.; Teyssandier, F.; Bancel, M.; Vallon, B. *Mater. Sci. Eng. A-Struct.* **1995**, *202*, 238.
- (14) Kato, A.; Tamari, N. *J. Cryst. Growth* **1980**, *49*, 199–203.
- (15) Dai, H.; Wong, E. W.; Lu, Y. Z.; Fan, S.; Lieber, C. M. *Nature* **1995**, *375*, 769–772.
- (16) Li, X. K.; Westwood, A.; Brown, A.; Brydson, A.; Rand, B. *Carbon* **2009**, *47*, 201–208.
- (17) Liu, X. G.; Zhang, S. W. *J. Am. Ceram. Soc.* **2008**, *91*, 667–670.
- (18) Liu, X. G.; Wang, Z. F.; Zhang, S. W. *Int. J. Appl. Ceram. Technol.* **2010**, *10*, 1111/j.1744-7402.2010.02529.x.
- (19) Li, X. K.; Yuan, G. M.; Westwood, A.; Zhang, H. B.; Dong, Z. J.; Brown, A.; et al. *Chem. Vap. deposition* **2008**, *14*, 40–45.
- (20) Walton, A. S.; Allen, C. S.; Critchley, K.; Górzny, M. L.; McKendry, J. E.; Brydson, R.; et al. *Nanotechnology* **2007**, *18*, No. 065204.
- (21) Craven, A. J.; Garvie, L. A. *J. Microsc. Microanal. Microstruct.* **1995**, *6*, 89–98.
- (22) Scott, A. J.; Brydson, R.; Mackenzie, M.; Craven, A. *J. Phys. Rev. B* **2001**, *63*, 245105, 6pp.
- (23) Williams, W. *JOM* **1997**, *49*, 38–42.
- (24) Wong, E. W.; Maynor, B. W.; Burns, D.; Lieber, C. M. *Chem. Mater.* **1996**, *8*, 2041–2046.
- (25) Li, X. K.; Yuan, G. M.; Brown, A.; Westwood, A.; Brydson, R.; Rand, B. *Carbon* **2006**, *44*, 1699–1705.